Contents lists available at ScienceDirect

Food and Bioproducts Processing

journal homepage: www.elsevier.com/locate/fbp

Modeling radio frequency heating of food moving on a conveyor belt

Jiajia Chen[b,c,*], *Soon Kiat Lau*[c], *Long Chen*[a,b], *Shaojin Wang*[a,d], *Jeyamkondan Subbiah*[b,c,**]

[a] *College of Mechanical and Electronic Engineering, Northwest A&F University, Yangling, Shaanxi 712100, China*
[b] *Department of Biological Systems Engineering, University of Nebraska-Lincoln, Lincoln, NE 68583, USA*
[c] *Department of Food Science and Technology, University of Nebraska-Lincoln, Lincoln, NE 68583, USA*
[d] *Department of Biological Systems Engineering, Washington State University, Pullman, WA 99164-6120, USA*

ARTICLE INFO

Article history:
Received 8 August 2016
Received in revised form 6 January 2017
Accepted 22 January 2017
Available online 1 February 2017

Keywords:
RF heating
Moving
Finite element model
Discrete moving step
Wheat
Lethal effect

ABSTRACT

A multiphysics model that coupled electric fields and heat transfer was developed to simulate the radio frequency (RF) heating of food moving on a conveyor belt. A discrete moving step approach was used in the simulation. The total power absorption increased considerably during the entry of the sample into the RF system, remained stable when the sample was fully covered by the top and bottom electrodes, and decreased when the sample moved out of the system. Edge and corner heating was observed from the power absorption distribution and electric field distribution. The model was validated by heating a rectangular container of wheat kernels moving on a conveyor belt in a RF system (27.12 MHz, 6 kW). The predicted spatial temperatures in top, middle, and bottom layers showed less than 3.5 °C lower prediction than the experimental result. The measured anode current showed a good linear correlation with the predicted total power absorption. The optimum number of discrete moving steps was determined to be nine for accurate temperature prediction with total conveyor belt movement distance of 1.13 m which is equivalent to optimize step size of 0.1256 m/step (0.3 m for entry and exit, respectively, and 0.53 m for fully covered by electrodes) at speed of 14.23 m h^{-1}. The movement of food product could help improve the heating uniformity of RF heating process.

1. Introduction

Electromagnetic heating is a non-traditional thermal processing method for its rapid and volumetric heating characteristics. Electromagnetic heating has been widely used for processing food, which involves interactions of electromagnetic waves with food products, such as radio frequency (RF) heating and microwave heating. Radio frequency waves are electromagnetic waves typically with a frequency range of kHz (Chen et al., 2016a) or MHz (Huang et al., 2015b) to 300 MHz (Datta and Anantheswaran, 2001). Because of higher penetration depth compared to microwaves due to relatively lower frequency and longer wavelength, RF heating is suitable for treating large bulk food products. RF heating process has shown potential in pasteurization of milk (Awuah et al., 2005), meats (Schlisselberg et al., 2013), and spices (Jeong and Kang, 2014; Kim et al., 2012); disinfestations in various agricultural commodities, such as chestnuts (Hou et al., 2014, 2015), walnuts (Mitcham et al., 2004; Wang et al., 2001), almonds (Wang et al., 2013), dried fruits (Alfaifi et al., 2014), fresh fruits (Birla et al., 2004, 2008; Wang et al., 2006), soybeans (Huang et al., 2015a), and wheat (Jiao et al., 2015); and thawing and cooking meat (Laycock et al., 2003;

* *Corresponding author at*: Department of Food Science and Technology, 249, Food Innovation Center, University of Nebraska-Lincoln, NE 68588-6205, USA.
** *Corresponding author at*: Department of Biological Systems Engineering and Food Science & Technology, University of Nebraska-Lincoln, 210 L.W. Chase Hall, NE 68583, USA.
E-mail addresses: jiajia.chen@unl.edu (J. Chen), Jeyam.subbiah@unl.edu (J. Subbiah).
http://dx.doi.org/10.1016/j.fbp.2017.01.009

Table 1 – Electrical, thermal, and physical properties of materials.

	Air[a]	Aluminum[a]	Wheat	Polypropylene[a]
Dielectric constant	1	1	4.3[b]	2.0
Dielectric loss factor	0	0	0.11[b]	0.0023
Electrical conductivity ($S\,m^{-1}$)	0	3.77×10^7	–	–
Density ($kg\,m^{-3}$)	–	–	860	900
Thermal conductivity ($W\,m^{-1}\,K^{-1}$)	–	–	0.15	0.2
Specific heat capacity ($J\,kg^{-1}\,K^{-1}$)	–	–	2670[b]	1800

[a] COMSOL Multiphysics (2015).
[b] Shrestha and Baik (2013).

Wang et al., 2012). The food products processed with RF heating also show higher (Fiore et al., 2013) or similar (Tang et al., 2005) nutritional values, and better functional properties (Boreddy et al., 2014, 2016) when compared to those products cooked conventionally. However, nonuniform heating is a big challenge for RF heating reported in these studies.

Computer simulation models have been developed as tools to understand and improve the heating uniformity of RF heating. Many factors that influence the heating uniformity in RF systems have been extensively studied, such as sample size, shape, position between the top and bottom RF electrodes, and dielectric properties of samples (Romano and Marra, 2008; Tiwari et al., 2011a; Uyar et al., 2014, 2015). Computer simulation model also has been developed to understand the effect of immersion of fruits in water to improve its heating uniformity (Birla et al., 2008). Jiao et al. (2014) developed a new strategy of placing polyetherimide (PEI) around peanut butter samples to improve the heating uniformity using modeling. However, these models only simulated the batch heating process where the products were placed at a stationary location between the top and bottom electrodes in the RF system.

Birla et al. (2004) developed a system to rotate and move the fruit in water when subject to RF heating, showed significant temperature uniformity improvement, even though it was still a batch process. In a real food industry application, it is more applicable to utilize the RF system for continuous processing of food products moving between the electrodes on a conveyor belt through the system. During the movement, the interactions between the food product and the RF system will change with time and the relative location of food in the system. A model that could simulate this continuous movement will help us understand the changing interaction and develop better processes to improve the RF heating performance. Chen et al. (2016a) developed a computer simulation model for RF heating of wheat considering the sample movement on a conveyor belt using an "equivalent power absorption" method. In this method, the power absorption of the food product at different locations in the RF system was determined by multiplying the power absorption at stationary condition (center of the RF system) with an arbitrary power ratio factor function. However, this method did not consider the change of the power distribution within the food product, which occurs when the food product is moving through the RF system. Therefore, a model that considers this power distribution change during the movement of products needs to be developed.

The movement (rotation) of food product in domestic microwave oven has been simulated in several studies (Chen et al., 2014, 2015, 2016b; Pitchai et al., 2015a,b) using discrete rotational steps. Instead of continuous rotation, food products were assumed to be rotated discretely on turntables. A similar approach of discrete moving steps could be utilized to simulate the translational movement of a food product in a RF system, which was also mentioned and discussed by Chen et al. (2016a). The more steps used, the closer is the simulation of movement to the actual "continuous" movement; however, more computational power or capacity may be needed. Therefore, it is necessary to determine the optimum number of moving steps to achieve accurate model prediction with acceptable computation time.

Therefore, the objectives of this study are to:

1) develop a 3-D numerical model that simulates RF heating with movement of food product on a conveyor belt using discrete moving step approach;
2) characterize the heating process to enhance the understanding of RF heating process with food product movement;
3) validate the model for RF heating of wheat kernel product moving on a conveyor belt; and
4) determine an optimum number of discrete moving steps that could provide accurate model predictions.

2. Materials and methods

In this study, a multiphysics based model was developed according to a reported and validated model that simulated RF heating of a stationary food product (wheat) placed at the center of the RF system (Chen et al., 2016a). The geometric model, material properties, governing equations, and initial and boundary conditions were obtained from this reported model (Chen et al., 2016a), which are also described briefly in the following sections.

2.1. *Sample preparation and material properties*

The wheat sample was obtained from a local farmer in Yangling, Shaanxi, China, and stored at 25 °C with relative humidity of 65% in a controlled chamber (BSC-150, Shanghai BoXun Industrial & Commerce Co., Ltd., Shanghai, China) prior to RF treatments. The initial moisture content of wheat was 8.7% (w.b.). During RF treatment, the wheat sample was placed in a rectangular container (inner dimension 300 mm × 220 mm × 60 mm). The thickness of the bottom and side walls of the container was 3 mm.

The electrical, thermal, and physical properties of materials (air, wheat sample, polypropylene container, and aluminum electrode base) used in the model are shown in Table 1.

2.2. *Physical model development*

2.2.1. *Geometric model and meshing scheme*

A 6 kW, 27.12 MHz parallel plate RF heating system with a free-running oscillator (COMBI 6-S, Strayfield International Limited, Wokingham, UK) was used in this study. The RF system was consisted of a metallic enclosure, a generator, and a RF applicator, as shown in Fig. 1(a). The applicator had a pair of parallel electrode plates, in which the top electrode can be adjusted to different heights to control the electrode gap between top and bottom electrodes. The bottom electrode was connected with the grounded metallic enclosure. The dimensions of the RF system and the food product are shown in Fig. 1(b).

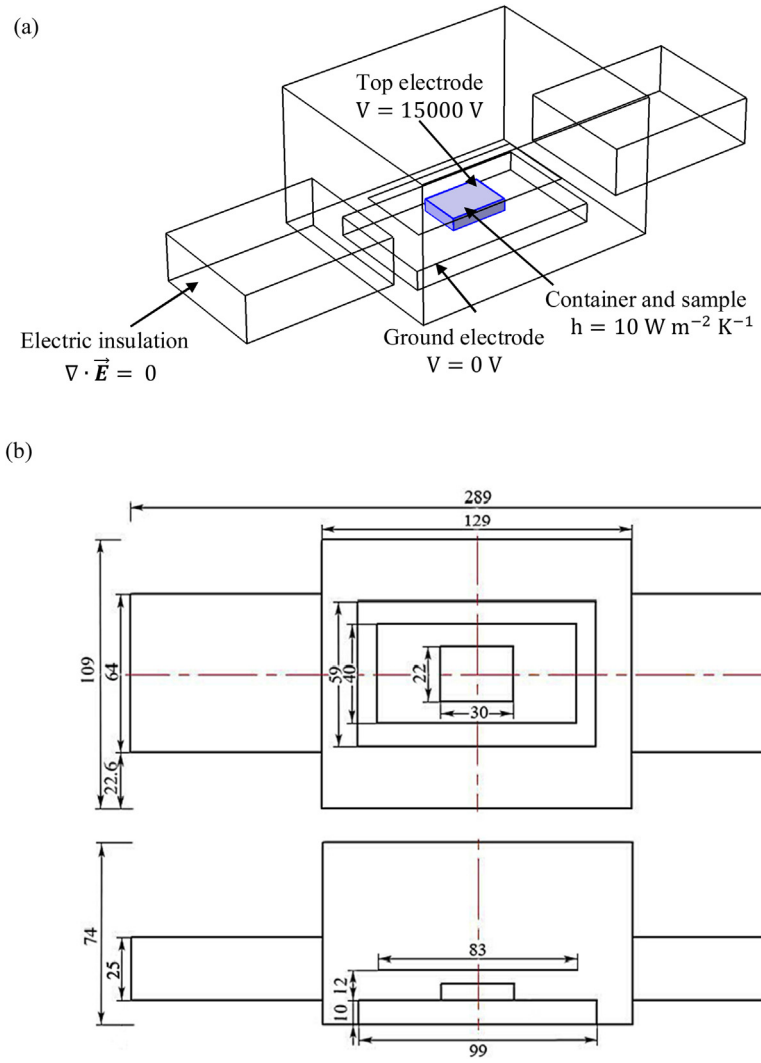

Fig. 1 – Three-dimensional scheme (a) and dimensions (b) of the 6 kW 27.12 MHz RF system and a container of wheat sample (dimensions in mm).

Following the approach described in Jiao et al. (2014), the mesh size was determined based on the independence mesh test when the difference of the maximum temperature between successive calculations was less than 0.1%. The meshes contained 79,906 domain (tetrahedral and pyramid) elements, 14,292 boundary (prism, triangular, and quadrilateral) elements, 837 edge elements and 56 vertex elements. The simulations were performed on a computer workstation with an available memory of 96 GB RAM running two twelve-core Intel Xeon E5-2667 processors at 2.9 GHz frequency (E2600, Microway Inc., Plymouth, MA).

2.2.2. *Governing equations*

The electric field in the RF system can be obtained from a quasi-static assumption of Maxwell's equations (Birla et al., 2008)

$$-\nabla \cdot ((\sigma + j2\pi f\varepsilon_0\varepsilon')\nabla V) = 0 \quad (1)$$

where $j = \sqrt{-1}$, ε' is the dielectric constant, σ is the electric conductivity (S m^{-1}) which is related to the dielectric loss factor ($\sigma = 2\pi f\varepsilon_0\varepsilon''$) (Guan et al., 2004), V is the electric potential across the electrode gap (V), f is the frequency (27.12 MHz), and ε_0 is the free space permittivity (8.854×10^{-12} F m^{-1}).

The electric field $\vec{E}$ (V m^{-1}) can be calculated as:

$$\vec{E} = -\nabla V \quad (2)$$

The amount of power converted from electromagnetic energy to thermal energy P (W m^{-3}) can be calculated as (Datta and Anantheswaran, 2001):

$$P = \pi f\varepsilon_0\varepsilon''|\vec{E}|^2 \quad (3)$$

The heat transfer in the food product and container is described by the Fourier's equation:

$$\frac{\partial T}{\partial t} = \frac{k}{\rho C_p}\nabla^2 T + \frac{P}{\rho C_p} \quad (4)$$

where $\frac{\partial T}{\partial t}$ is the instantaneous heating rate of the food product (K s^{-1}), k is the thermal conductivity (W m^{-1} K^{-1}), ρ is the density (kg m^{-3}), and C_p is the specific heat capacity (J kg^{-1} K^{-1}).

The electromagnetic heat source is not generated in the air domain. Because the ambient air temperature increase is negligible, a convective heat transfer boundary was used to consider the heat transfer between food product and air. Thus, the heat transfer equation was only solved for food and container in this study. The temperature profiles in the food

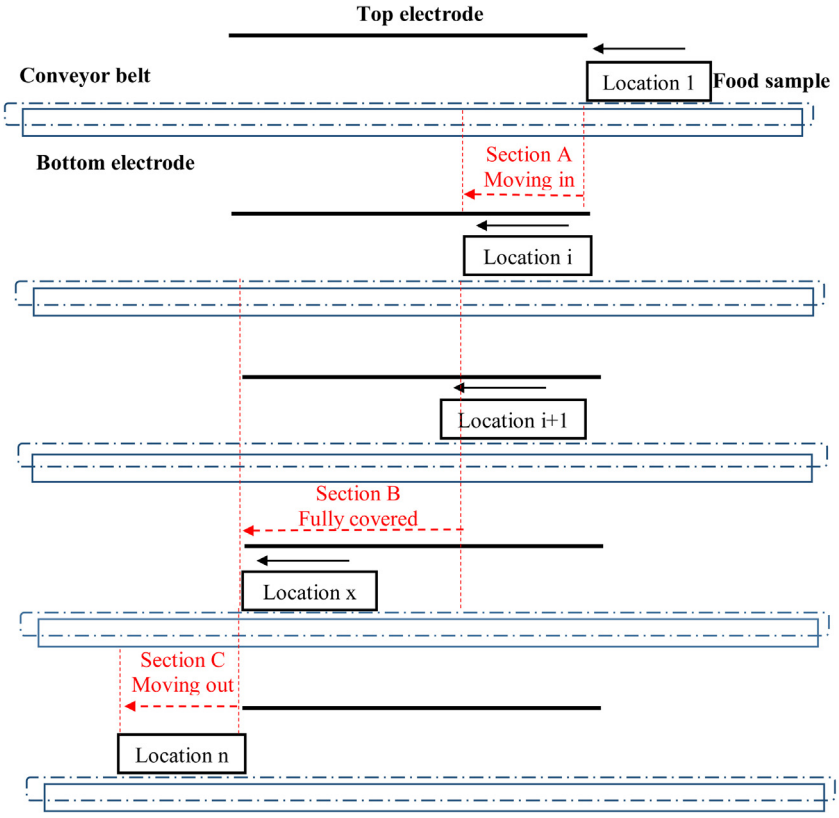

Fig. 2 – Discrete movement of the food product on a conveyor belt in the RF system with n moving steps (locations).

product and container were obtained by simultaneously solving Eqs. (1)–(4).

2.2.3. *Initial and boundary conditions*

The initial temperature (T_0) of the food product and PEI container was set as 25 °C. The boundary conditions of the model are shown in Fig. 1(a). The potential of the top electrode was set at 15,000 V (Chen et al., 2016a) which was estimated by matching the simulation results with experimental heating rate proposed by Birla et al. (2008). The bottom electrode and the metallic enclosure were set as ground (Jiao et al., 2014).

The open faces of the inlet and outlet tunnels of the RF system were set as electric insulation:

$$\nabla \cdot \vec{E} = 0 \quad (5)$$

The outer surface of the container and top surface of food product were exposed to air (25 °C) with a convective heat transfer coefficient (Pitchai et al., 2014):

$$h = 10\,W\,m^{-2}\,K^{-1} \quad (6)$$

2.2.4. *Simulation strategy*

A commercial finite element method based software COMSOL Multiphysics (V5.2 COMSOL Multiphysics, Burlington, MA, USA) was used to simulate the RF heating process with the movement of food product. The food product was placed on a conveyor belt with a moving speed, $u = 14.23\,m\,h^{-1}$.

Chen et al. (2016a) used an equivalent power absorption approach to simulate the RF heating of a moving sample. First, the power density was calculated for a stationary RF heating process where the food product was placed at the center of the RF system. During entry and exit, the product is not completely exposed to the electrodes and therefore the electromagnetic waves. Only a fraction of the product surface area is exposed. The authors used an arbitrary power ratio function, which is a cubical rather than linear. No explanation for selection of cubical function was given by Chen et al. (2016a). The magnitude of power density of the product, when it was stationary at the center, was then adjusted by the arbitrary power function for power density of product during the whole movement. When the product was not covered by the top and bottom electrodes, the power ratio was set as 0; when the sample was fully covered by the top and bottom electrodes, the power ratio was set as 1; when the sample was moving into or out of the RF system (partial of the product was covered by top and bottom electrodes), a cubical function with values between 0 and 1 was used. During entry and exit, this method assumed that heating occurs in all areas of the product with a pattern similar to that at the center. However, in reality, the heating would vary spatially based on where the product is exposed to electrodes.

In this study, a discrete movement approach was used to simulate the movement of wheat sample on the conveyor belt, as shown in Fig. 2. At time t = 0 s, the wheat sample was placed at the right side of the system, where the left side of the sample was just below the right end of the top electrode. Then, the food product was moved to the left direction into the RF system. The whole moving process can be divided to three sections. Section A is where the sample was moved into the system and part of the sample was covered by the top and bottom electrodes; section B is where the sample was fully covered by the top and bottom electrodes; section C is where the sample was moved out of the RF system and part of the sample was covered by the top and bottom electrodes.

A custom routine was developed to interface COMSOL Multiphysics with MATLAB (MathWorks Inc., Natick, Massachusetts) to simulate the food movement as shown in Fig. 3. The Electric Current module and Heat Transfer in Solids

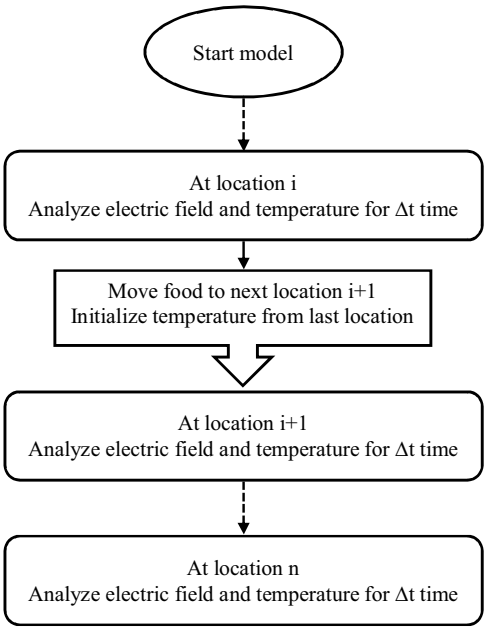

Fig. 3 – Flow chart depicting modeling of RF heating with discrete movement of food product (i = 1 to n-1).

module were coupled to solve the electromagnetic and heat transfer equations simultaneously. At location i, the sample was assumed to be heated at that stationary location for a period time of Δt. Then the sample was moved to the next location $i+1$ for another heating period of Δt. The distance between two adjacent locations $\Delta L = \Delta t\, u$. At location i, the electric field distribution and temperature were simultaneously solved; when the sample was moved to location $i+1$, the sample temperature was initialized by the solution from location i, and the electric field and temperature distribution were solved again. This movement of product, initialization, and equations solving steps were repeated until the last location n was completed. This method would predict different heating distribution during the whole movement process, including entry and exit locations.

2.3. Model evaluation and validation

2.3.1. Characterization of RF heating process

In this discrete moving step approach, an arbitrary and a large number of moving steps (25) was used in the developed model. This model was used as a baseline model to characterize the RF heating process using parameters, such as total power absorption, power density distribution, and electric field distribution. The total power absorption values of the food sample at different (movement) locations were evaluated by integrating the power density over the whole volume of the food. Nodal power densities at various spatial nodes inside the food product for a specific movement location in the RF oven were correlated with the corresponding nodal power densities at the center of RF oven. The coefficient of determination values (indicating the linear relationship between two variables) were obtained to understand the change of power density distribution in the food product with time and locations in the RF system. The coefficient of determination (R^2) can be calculated as:

$$R^2 = \left(\frac{\sum_i (x_i - \bar{x})(y_i - \bar{y})}{\sqrt{\sum_i (x_i - \bar{x})^2} - \sqrt{\sum_i (y_i - \bar{y})^2}} \right)^2 \quad (7)$$

where x_i and y_i are the nodal power densities predicted by the two models for comparison at node i, $\bar{x}$ and $\bar{y}$ are average values of the power densities predicted by two models.

The volumetric and sliced power density distributions and electric field distributions were also visualized at different locations to understand the RF heating process.

2.3.2. Model validation

About 3.39 kg of wheat filled in a rectangular polypropylene container was placed on the conveyor belt with a moving speed (u) of 14.23 m h^{-1}. The sample was heated in a RF system for 287 s (moved from location 1 to location n as shown in Fig. 2) to validate the model. The anode current is the current that flows in the triode valve in the RF system, which is virtually related to the RF power absorbed by the product. The anode current of the RF system during the entire RF heating process was recorded and compared with the predicted power absorption. Two thin polypropylene films were placed in the container to separate the sample to three layers, so that the thermal images can be acquired at multiple layers. After the RF heating process, the spatial temperature profiles in top, middle, and bottom layers (60, 40, and 20 mm from the bottom of the container, respectively) were recorded by an infrared camera (DM63-S, DaLi Science and Technology Co., LTD, Zhejiang China) with an accuracy of ±2 °C. The details of model validation can be found in Chen et al. (2016a). The predicted results using discrete moving step approach in this study were also compared with those using equivalent power absorption approach reported by Chen et al. (2016a).

2.3.3. Determination of optimum discrete moving steps

An arbitrary and a large number of moving steps (25) was used in the discrete moving step approach. Larger number of moving steps would improve accuracy, but requires longer computation time. Therefore, an optimum number of moving steps needs to be determined. The model using 25 discrete moving steps was used as a baseline one. Models with smaller discrete moving steps (5–23) were developed similarly as "simpler models". The nodal volumetric temperature predicted by the simpler models was then compared to that of the baseline model to determine the coefficient of determination using Eq. (7). The root-mean-square error (RMSE) values of nodal temperatures between the simpler models and the baseline model were calculated to quantify the temperature prediction accuracy. The optimum number of discrete moving steps was determined from the coefficient of determination and RMSE.

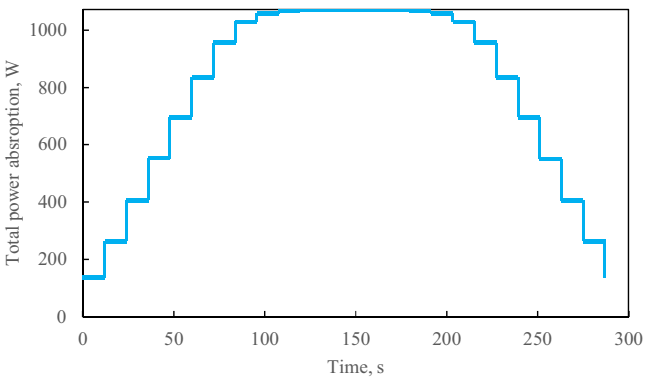

Fig. 4 – Predicted total power absorption of food moving on a conveyor belt with 25 discrete moving steps during 287 s heating process with an electrode gap of 120 mm.

2.3.4. *Determination of heating nonuniformity index*

The average and standard deviation of the volume temperature of the food product were evaluated. The heating nonuniformity index (coefficient of variation) can be determined as:

$$\text{Heating nonuniformity} = \text{standard deviation/average temperature} \quad (8)$$

3. Results and discussions

3.1. *Characterization of RF heating process*

3.1.1. *Total power absorption*

The total power absorption of the food product during the RF heating process with movement of package on the conveyor belt is shown in Fig. 4. At time t = 0 s, the total power absorbed by the food product was about 136 W, even though the food product was not covered by the top electrode. At this time, the food product was just out of the coverage of the top electrode, where the electric field fringing from the edge of the top electrode barely entered the edge of the food product. The total power absorption was maintained at a constant value for a period of time Δt where the food product was assumed to be heated for time of Δt at that location. When the food product was moved to the locations between the top and bottom electrodes gradually, the total power absorption of the food product increased considerably in a stepped manner. This stepped changing of total power absorption was attributed to the discrete moving steps of food product where the food product was not continuously moving on the conveyor belt. When the food product was moved to the location where the food product was totally covered by the top and bottom electrodes, the total power absorption was around 1050 W, which did not change considerably after that. The total power absorption reached the maximum value of 1072 W at the center of the RF system (location 13). When the food product was at the center of the system (location 13), the ratio of total absorbed power to the output power was 17.8% (1072/6000). Romano and Marra (2008) studied the effect of product shape and dielectric properties (loss tangent) on power absorption, and found that the ratio of total absorbed power to the output power ranged from 2% to 50% for different shapes of products. Cube products typically absorbed 40%–50% of the output power, which was higher than the one reported in this study. This may be attributed to the higher ratio of sample surface to the electrode surface in Romano and Marra (2008). Romano and Marra (2008) also reported that the food product with higher loss tangent value showed higher power absorption ratio. The lower loss tangent ratio of wheat (0.026) in this study may also have contributed to the low power absorption ratio. The total power absorption showed symmetric shape with time (Fig. 4), which was attributed to the constant dielectric properties used in the model. The total power absorption was only dependent on the relative location of the sample in the RF system. If moisture- and temperature-dependent dielectric properties are used, the total power absorption will not only change with the relative location, but also change with time (usually increase with time because of increasing dielectric loss factor with increase in temperature).

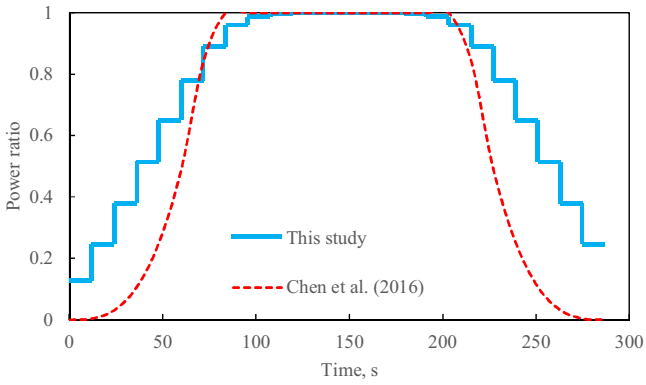

Fig. 5 – Comparison of power ratio (ratio of total power absorption at different locations during food moved on the conveyor belt to that at the center location) between the discrete moving step approach in this study and the equivalent power absorption approach used in Chen et al. (2016a).

The power ratio, defined as the power absorption in the whole volume of the sample at a given movement location to the power absorption at the center of the RF system, is shown in Fig. 5. The arbitrary power ratio function used in Chen et al. (2016a) showed considerable difference from the power ratio curve evaluated by the model in this study. At time t = 0 s, the power ratio in Chen et al. (2016a) was set as 0; but the power ratio in this study was about 0.13 indicating that the food product absorbed some amount of power. The power ratio also showed big difference in the moving in section (Section A) when the food product moved from t = 0 s to the locations where the food product was fully covered by the top and bottom electrodes (location 8). In the fully covered section (Section B), the total power absorption did not show a big difference. These differences in total power absorption may cause prediction accuracy issues for the model reported by Chen et al. (2016a). However, for a RF system with long electrodes, which has a long heating duration in Section B, the heating effect of Sections A and C might be minimum and negligible.

3.1.2. *Power absorption density during movement of food product*

During the movement of the sample in the RF system, the total power absorption changed with location and time, and so did the power absorption density distribution within the food product, especially when the food product was not fully covered by the top and bottom electrodes. The volume and sliced power density distribution in the food product at different locations (locations 1, 4, 7, 8, and 13) are shown in Fig. 6. At location 1, the food product was just on the right edge of the top electrode, where the food product was not covered by the top electrode. The left edge of the sample absorbed a small amount of electric power, which was also observed from the total power absorption (Fig. 4) and the power ratio (Fig. 5). When the food product was moved to the locations where the food product was partially covered by the top electrode, the covered part absorbed most of the energy. Even at location 7 where only the right edge of the sample was not covered, the outside part of the sample did not absorb much energy. After the food product was fully covered by the top electrode, the power distribution within the food product did not show considerable difference as seen in location 8 (totally covered) and

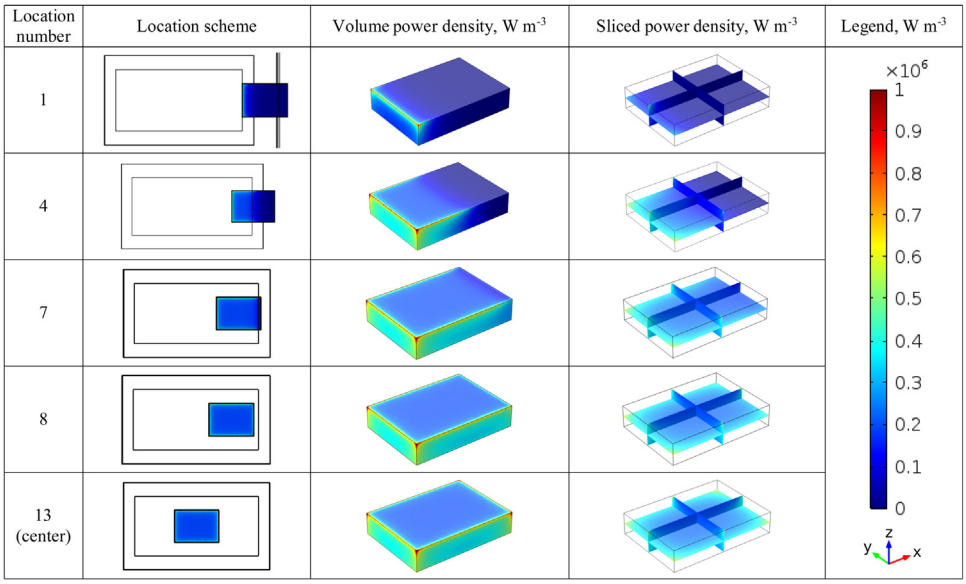

Fig. 6 – Predicted volume and sliced power density distributions in the food product at different locations during the movement of food on a conveyor belt with an electrode gap of 120 mm.

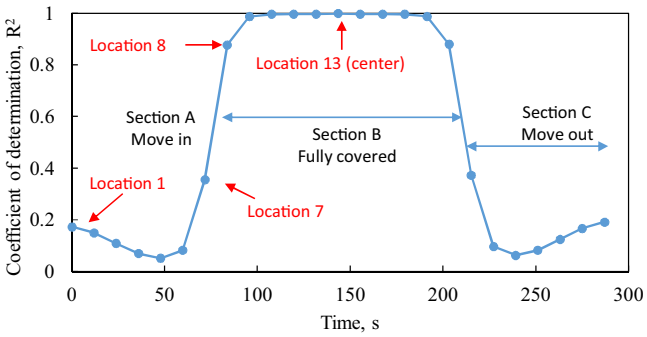

Fig. 7 – Coefficient of determination (R^2) of nodal volumetric RF power densities between that at 25 discrete locations and that at the center location.

location 13 (at the center of the RF system). The power absorption profiles during exit are flipped version of those during entry. The edge and corner heating phenomenon also can be clearly observed from the volume power density distribution, even when the food product was moved to the center of the RF system. This also has been observed in many other studies where the food products were placed at the center of the RF system without movement, such as RF heating of walnuts (Wang et al., 2007), dry fruit (Alfaifi et al., 2014), wheat flour (Tiwari et al., 2011b), and frozen meat (Uyar et al., 2014, 2015).

To further understand the change of power density distribution within the food product during the food product moving into the RF system, the nodal volumetric power density of the food product at different locations was correlated to that of the food product at the center of the RF system (location 13). The coefficient of determination is shown in Fig. 7. The coefficient of determination in Section A (moving in Section) was as low as 0.05 at location 5; even when the food product was moved to location 7 where the food product was almost fully covered by the top and bottom electrodes, the coefficient of determination was about 0.36. After the food product was moved to the locations where the food product was fully covered by the top and bottom electrodes (Section B), the coefficient of determination increased to 0.88 (locations 8 and 18) and mostly remained in the range of 0.99 and 1 (locations 9–17). After that, the food product began exiting the electrodes (Section C) and the coefficient of determination dropped considerably and showed similar values to those of Section A. Chen et al. (2016a) assumed that the power ratio was 1 when the food product was fully covered by the top and bottom electrodes, which was reasonable, as shown in Figs. 5 and 7. However, the low coefficient of determination values in Sections A and C showed that the equivalent power absorption approach used in Chen et al. (2016a) would introduce considerable prediction error in the model. Therefore, this discrete moving step approach in this study could properly incorporate the power distribution change during the movement of food product in the RF system into the model.

3.1.3. *Electric field distribution during movement of food product*

In addition to the total power absorption and power absorption density distribution, the model also can be used to visualize the spatial electric field distribution inside the food product, so that the RF heating process can be further understood. Fig. 8 shows the electric field pattern within the food product (z–x plot) at different locations (locations 1, 4, 7, 8, and 13) during the movement of the food product into the RF system. The arrow direction indicates the electric field direction while the color of the arrow indicates the magnitude of the electric field density. At time t = 0 s (location 1), the electric field between the top and bottom electrodes was distorted by the food product due to fringe effects, even though the food product was not between the top and bottom electrodes. This is because the food product has a relatively larger dielectric loss factor (electric conductivity) when compared to air. The food product showed lower resistance compared to the air and formed a current loop between top and bottom electrodes. When the food product was moved to the places between top and bottom electrodes, the electric field around the edges of the food product had higher electric field magnitude due to fringe effect. This concentration of electric field on the edges of the food product resulted in the higher power density distribution, which was observed in Fig. 6. This increase in magnitude of electric field on the edges of food product has also been reported by Jiao et al. (2014). Based on the electric field pat-

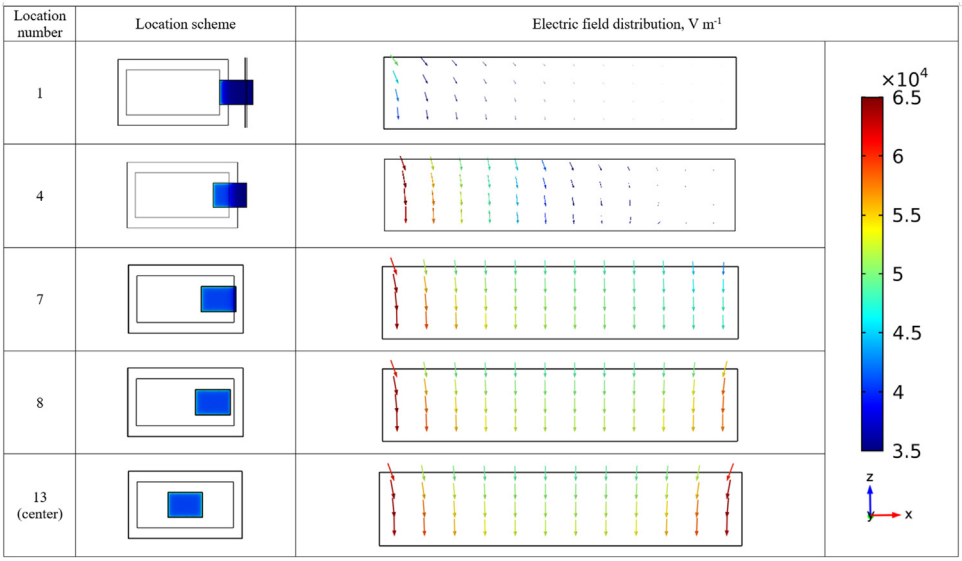

Fig. 8 – Predicted sliced (x–z plot) electric field distribution in the food product at different locations during the movement of food on a conveyor belt with an electrode gap of 120 mm (arrows indicates electric field direction; color indicates magnitude of the electric field).

tern predicted by simulation, Jiao et al. (2014) developed a new strategy of placing PEI around peanut butter samples. The fringe effect of electric field happened on the edges of PEI instead of food sample, so that the heating uniformity was improved.

3.2. *Model validation*

3.2.1. *Temperature*

The spatial temperature profiles (average ± spatial standard deviation) in the top, middle, and bottom layers from experiment and simulation in this study (with 25 moving steps) and Chen et al. (2016a) are shown in Fig. 9. Note that, the standard deviation values were that for spatial temperature distribution, not for replications. Generally, the spatial temperature predicted by the models in different layers matched well with the experimental data. The edge and corner heating can be observed for all the three layers, which has been discussed in Sections 3.1.2 and 3.1.3. The top layer temperature obtained from experiment was higher than that of simulation results. In this study, the simulated average temperature in the top layer was about 3.5 °C lower than the experimental value. This may be attributed to a thin layer of plastic mesh covering the top surface of sample in the experiment, which reduced the heat loss on the surface (Chen et al., 2016a). The simulation results in middle and bottom layers showed a good agreement with the experimental ones. The difference between simulation and experiment may also be attributed to the constant material properties at a single temperature and moisture content used in the model. In reality, the dielectric, thermal, and physical properties of food product are usually temperature and moisture dependent (Chen et al., 2013; Sipahioglu and Barringer, 2003).

The simulated temperatures in three layers using discrete moving step approach in this study were higher than those using equivalent power absorption approach reported by Chen et al. (2016a), showing better match with the experimental ones. This is mainly because the arbitrary function of power ratio used in Chen et al. (2016a) under predicted the power absorption (Fig. 5) and therefore the temperature. Therefore, it is critical to simulate heating performance at the entry and exit locations of food product in the RF system. Note that, the model using equivalent power absorption approach was redeveloped in this study and showed different predicted temperatures when compared with the results also using equivalent power absorption approach in Chen et al. (2016a). In Chen et al. (2016a), a convective heat transfer was applied on the food surface as boundary, which was not taken effect because the heat transfer equation was solved for all the domains of food, container, and air. Also in the post-processing of the modeling results, Chen et al. (2016a) exported the nodal temperatures from the model and calculated the average temperature based on these nodal temperatures. This average temperature was not accurate, because the volume sizes of elements were different which was not considered in the calculation. In this study, the average temperature was evaluated in the model itself where the volume sizes of elements were considered by weighted average based on volume. These differences caused the slight difference in predicted temperatures of equivalent power absorption approach between the model in Chen et al. (2016a) and the model redeveloped in this study.

In this study, constant dielectric properties were used. If moisture- and temperature-dependent dielectric properties are used, the equivalent power absorption approach will introduce more errors than the discrete moving step approach. As shown in Fig. 9, the discrete moving step approach results in improved heating uniformity with lower spatial standard deviation, when compared to the equivalent power absorption approach. Because the dielectric loss factor increases with increase in temperature, hot spots tend to heat faster than the cold spots. The equivalent power absorption approach would result in exasperated “run-away” heating effect than the discrete moving step approach. Thus, if more accurate moisture- and temperature-dependent properties are incorporated, the discrete moving step approach should result in better prediction than the equivalent power absorption approach.

3.2.2. *Anode current*

The anode current during the RF heating process with movement of the food product is shown in Fig. 10. The anode current increased considerably from 0.315 A to 0.400 A for about the

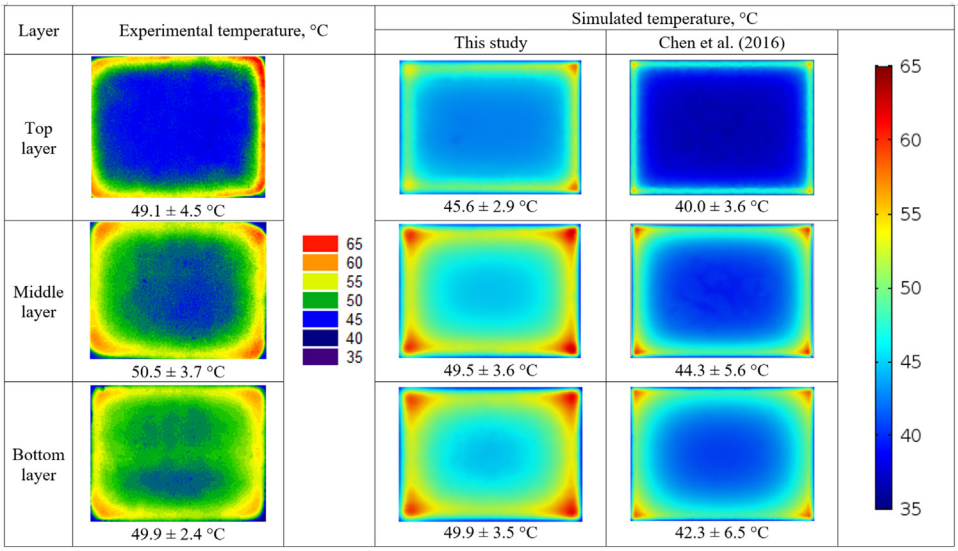

Fig. 9 – Comparison of spatial temperature profiles and average ± standard deviation values in top, middle, and bottom layers (60, 40, and 20 mm from the bottom of the sample) after 287 s RF heating with movement between the experiment and models in this study and Chen et al. (2016a).

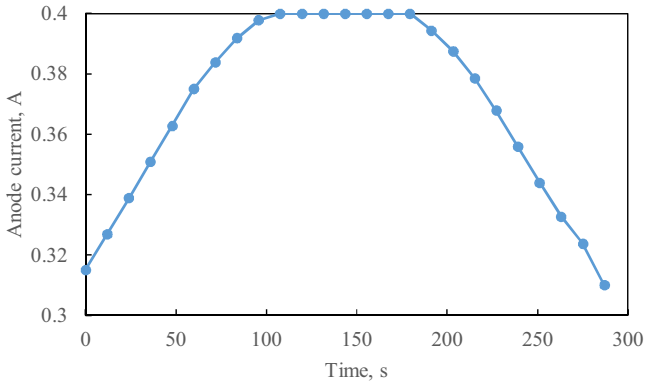

Fig. 10 – Measured anode current during the RF heating process with the food product moved with a speed of 14.23 m h^{-1} and an electrode gap of 120 mm.

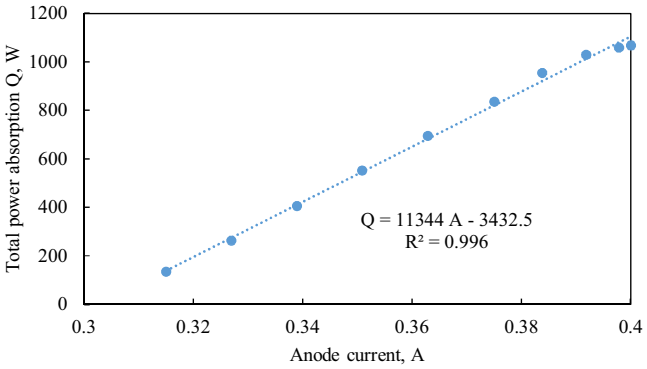

Fig. 11 – Correlation between the predicted total power absorption (Q) of the food product and the measured anode current (A) during the RF heating process with the food product moved with a speed of 14.23 m h^{-1} and an electrode gap of 120 mm.

first 100 s, which corresponds to the period of moving in section (Section A) when the food product was moved into the locations between top and bottom electrodes. Then the anode current remained almost constant at 0.400 A in fully covered section, until the food product was moved out of the system where the anode current decreased gradually. Jiao et al. (2012) measured the anode current in a RF heating system with movement of 8 containers of lentils, and reported similar results. The anode current in the stable region was about 1.2 A, which was higher than that in this study. This might be attributed to the larger amount of sample (8 containers with dimension of 400 × 230 × 100 cm^3 each) used in Jiao et al. (2012), where the food product fully filled the space between the top and bottom electrodes. A relatively smaller sample (1 container with dimension of 300 × 220 × 60 mm^3) was used in this study.

The measured anode current was correlated with the total power absorption predicted by the simulation model, as shown in Fig. 11. The total power absorption linearly increased with the measured anode current with $R^2 = 0.996$, showing good correlation between the predicted total power absorption and the measured anode current. Similar linear correlation has been obtained and reported based on experimental studies (Jiao et al., 2012; Wang et al., 2007).

3.3. *Determination of optimum number of moving steps*

The coefficient of determination and RMSE values between the nodal temperatures predicted by the simpler models using different discrete moving steps and the baseline model using 25 steps are shown in Fig. 12. The coefficient of determination increased with the number of moving steps (locations) and remained stable, showing better temperature prediction with more moving steps. Thus, it can be confirmed that the model using 25 discrete steps could provide accurate power absorption and therefore temperature prediction. The RMSE values decreased when the number of moving steps (locations) increased. The coefficient of determination increased to 0.99 and the RMSE value decreased to 0.47 °C when 9 moving steps (locations) were used in the model, indicating that the model using 9 moving steps does not show considerable difference with the model using 25 moving steps. This error of temperature prediction falls within the typical temperature

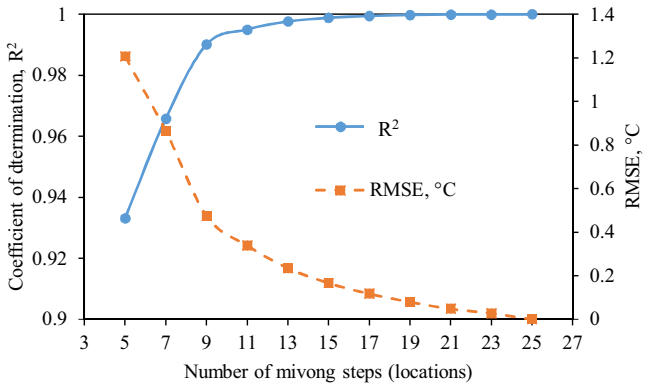

Fig. 12 – Coefficient of determination and root mean square error of nodal temperature between the "base model" using 25 discrete moving steps and the "simpler models" using different number of moving steps.

Table 2 – Coefficient of determination and root mean square error of volume nodal temperature between the model using 25 discrete moving steps and those using 9 discrete moving steps uniformly and not uniformly distributed on the conveyor belt.

Parameter	Locations uniformly distributed (9)	Locations not uniformly distributed (9)
Coefficient of determination (R^2)	0.9900	0.9904
RMSE (°C)	0.474	0.466

measurement error using thermocouples. Therefore, 9 moving steps might be enough to achieve accurate simulation result.

As shown in Figs. 6 and 7, the power density distribution within the food product changed considerably when the food product was moved into and out of the areas between top and bottom electrodes, but did not change much when the food product was fully covered by the top and bottom electrodes. Therefore, the electric field might not need to be calculated too frequently when the food product is fully between the top and bottom electrodes; instead it is better to calculate more steps when the food product is moving into and out of the electrodes. For example, 4 discrete steps can be used when the food product was moved both into and out of the electrodes areas, and only one step can be calculated at the center. In this study, this strategy with 9 locations of food product not uniformly spaced along the whole movement range was evaluated. This nonuniform step was compared to its uniformly-spaced counterpart and the results are shown in Table 2. This new approach of 9 nonuniformly distributed steps showed slightly higher coefficient of determination and lower RMSE values than the approach of 9 uniformly distributed steps, showing better model prediction results. However, the difference between these two approaches did not show considerable difference. Therefore, it might be good enough to simulate the moving process with 9 uniformly distributed steps during the whole moving process.

Computation time is also one important parameter that needs to be considered for determining the optimum number of steps (locations). Liu et al. (2013) studied the number of rotational steps of food product in a microwave heating process with rotation of turntable, and found that it was enough to use 12 rotational steps to achieve accurate model prediction and acceptable simulation time. Because of high computational power needed in the microwave heating simulation, the effect of model setups, such as modeling coupling, temperature-dependent properties updating, etc., on model prediction accuracy and computation time have been systemically studied (Chen et al., 2015). The computation time of modeling microwave heating process can be reduced from 60 h to 4 h (93% reduction) by using dielectric properties at room temperature without updating. In this study, RF heating modeling is relatively low in computation time (in the order of minutes, about 18 min for 9 steps and 40 min for 25 steps) when compared to microwave heating process (in the order of hours). Therefore, it might be acceptable to use more moving steps during the whole moving process to simulate the RF heating process with movement of food product. However, it will be necessary to determine the optimum number of moving steps for a computationally intensive model, such as a RF heating model that incorporates mass transfer physics and/or fluid flow to predict the moisture profiles within the food product.

The strategy of calculating one location when the food product was fully covered by the top electrode can be used to simplify the simulation process and save computation time considerably, especially for the RF heating system with a much longer electrode. Further, if the top electrode is long enough, which means the time for the food product moving through the electrodes (Section B) is much bigger than that the food product move into and out of the system (Sections A and C), a stationary model may be good enough to predict the performance of RF heating. Note that the discussion above was made based on the simulation using constant dielectric properties in the model. If the dielectric properties of food change considerably during the RF heating process, the power density distribution may change considerably, which may require more frequent moving steps to update the temperature and moisture dependent dielectric properties. But the findings from this study are valid for the food product with relatively constant dielectric properties during the RF heating.

3.4. *Effect of movement on heating performances*

The effect of movement of food product (with different moving velocity or heating time) on the heating performances (maximum, minimum, average, and spatial standard deviation temperatures and heating nonuniformity, as measured by coefficient of variation) were shown in Fig. 13. The heating nonuniformity indices were determined as standard deviation/average temperature (Eq. (8)). The stationary product would have heated 10.2 °C higher than the product moving on a conveyor belt through the RF electrodes with same heating time (287 s). This was because the food product was not fully heated for the period of time when the food product was moving into and out of the RF system. The stationary food product also showed higher spatial temperature variation with standard deviation of 3.0 °C higher than the moving food. Thus, the calculated nonuniformity of stationary food was about 3.6% higher than that of moving food. The food product can be heated to a higher temperature if the food product was moving slower through the system. For example, when the moving velocity was reduced to 8.13 m h^{-1} (the heating time was 487 s), the average temperature can be increased to 64.0 °C which was higher than that of stationary condition. The standard deviation and nonuniformity were still lower than those of stationary scenario. Therefore, the movement of food prod-

Table 3 – Final temperature at the coldest spot in the heated sample and the cumulative thermal mortality at different heating conditions.[a]

Parameter	S-287 s	M-287 s	M-487 s	M-584 s	M-778 s	M-973 s
Final temperature at coldest spot (°C)	33.5	36.6	45.8	50.0	58.0	65.5
Cumulative thermal mortality	0%	0%	0%	1%	100%	100%

[a] S for stationary, M for Moving, numbers indicate the heating time in seconds.

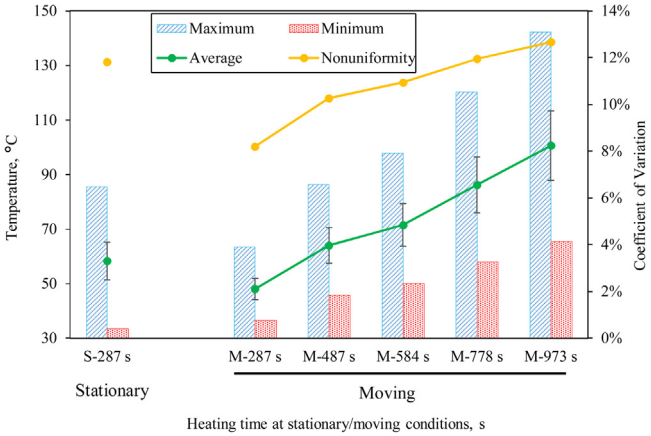

Fig. 13 – The effect of movement of food product (with different moving velocity or heating time) on the heating performances (maximum, minimum, average, and spatial standard deviation temperatures and coefficient of variation (heating nonuniformity)). S for stationary, M for moving.

uct through the RF system could help improve the RF heating uniformity.

The insects in wheat sample can be killed in less than 1 min if the sample is heated above 62 °C (Tang et al., 2007). In this study, the minimum temperature of both scenarios of heating at stationary and moving conditions for 287 s did not reach the lethal temperature. However, the moving velocity of the conveyor belt can be reduced to increase the heating time, so that the sample can be heated to the desired lethal temperature. For example, if the moving velocity was adjusted to 4.18 m h^{-1} with heating time of 973 s, the minimum temperature can reach 65.5 °C, which could meet the requirement of insect control. In reality, lethal effect of the RF heating process depends on the transient temperature of the sample. If the inactivation kinetics of insects is available, the predicted transient temperature can be used to determine the cumulative lethal effect. For example, a 0.5 order thermal death kinetics model of red flour beetle was developed by Johnson et al. (2004), as shown in Eqs. (9) and (10).

$$\frac{d\left(\frac{N}{N_0}\right)}{dt} = -k\left(\frac{N}{N_0}\right)^{0.5} \quad (9)$$

$$k = 130.21–42.52 \times 1000/T \quad (10)$$

where N_o and N are the initial and surviving numbers of insects, t is the exposure time (min) at a fixed temperature, k is the thermal death rate constant (1/min).

Combining with the transient point temperature at the coldest location in the heated sample, the thermal mortality of red flour beetle at different heating conditions was shown in Table 3. The thermal mortality was only 1% after 584 s with continuous movement of conveyor, because the final temperature was only heated to 50.0 °C at the coldest spot which is much lower than the lethal temperature; while thermal mortality reached 100% after 778 s heating, where the coldest temperature reached near lethal temperature. The model can be used to modify electrode and product shape to minimize heating nonuniformity which would result in insect control with minimal deterioration of the sample quality.

3.5. *Potential applications of this model in industry*

This model simulated the RF heating of a food product moving on a conveyor belt through a RF system, which is closer to the real food industry applications of RF heating process. This model can be used to understand and improve the industrial continuous RF heating of food products, so that more uniform heating can be achieved. The stable power density distribution within the food product when the food product was fully covered by the top and bottom electrodes showed that, the developed novel simulation strategy can be used to simplify the simulation. This could help save computation time considerably, especially for modeling of RF heating with a long electrode.

4. Conclusions

A 3-D multiphysics based computer simulation model was developed to simulate the RF heating of a food product moving on a conveyor belt. A discrete moving step approach was used to simulate the movement of the food product. The model using 25 discrete locations (steps) uniformly distributed on the conveyor belt was used as a baseline one to understand the power absorption, electric field, and temperature distribution in the RF heating process. The total power absorption increased considerably when the food product was moved into the system, remained stable when the food product was moved between the top and bottom electrodes, and decreased when the food product was moved out of the system. Edge and corner heating was observed for the whole heating process and attributed to the distortion of electric field at the edges of the food product. The model was validated by heating of a container of wheat sample in a RF system (27.12 MHz, 6 kW) for 287 s with the conveyor speed of 14.23 m h^{-1}. The predicted spatial temperature in top, middle, and bottom layers of the wheat sample showed a good agreement with the experimental results. The measured anode current showed a linear correlation ($R^2 = 0.996$) with the predicted total power absorption, indicating a good model prediction. It was determined that the model with 9 discrete locations uniformly distributed on the conveyor belt with total movement distance of 1.13 m (0.3 m for entry and exit, 0.53 m for fully covered by electrodes) and speed of 14.23 m h^{-1} could achieve accurate temperature prediction. If the residence time of product under the electrode is significantly longer compared with the time of entry and exit, a simple stationary model might be sufficient. However, temperature dependent properties might affect the model prediction and require more moving steps. As computation time

in modeling RF heating is not too high, it is better to simulate conveyor movement using more moving steps to achieve more accurate model prediction. The movement of food product through RF system can help improve the heating uniformity when compared to the stationary treatment. This model can be used to understand and improve the RF heating process with food product continuously moving on a conveyor belt.

Acknowledgements

This research was supported by the USDA hatch project NEB-21-162 and USDA NIFA Award 2014-67005-21734.

References

Alfaifi, B., Tang, J., Jiao, Y., Wang, S., Rasco, B., Jiao, S., Sablani, S., 2014. Radio frequency disinfestation treatments for dried fruit: model development and validation. J. Food Eng. 120, 268–276, http://dx.doi.org/10.1016/j.jfoodeng.2013.07.015.

Awuah, G.B., Ramaswamy, H.S., Economides, A., Mallikarjunan, K., 2005. Inactivation of *Escherichia coli* K-12 and *Listeria innocua* in milk using radio frequency (RF) heating. Innov. Food Sci. Emerg. Technol. 6, 396–402, http://dx.doi.org/10.1016/j.ifset.2005.06.002.

Birla, S., Wang, S., Tang, J., Hallman, G., 2004. Improving heating uniformity of fresh fruit in radio frequency treatments for pest control. Postharvest Biol. Technol. 33, 205–217, http://dx.doi.org/10.1016/j.postharvbio.2004.02.010.

Birla, S.L., Wang, S., Tang, J., 2008. Computer simulation of radio frequency heating of model fruit immersed in water. J. Food Eng. 84, 270–280, http://dx.doi.org/10.1016/j.jfoodeng.2007.05.020.

Boreddy, S.R., Birla, S., Froning, G., Thippareddi, H., Subbiah, J., 2014. Effect of radio frequency assisted thermal processing on quality and functional properties of egg white powder. Trans. ASABE 57, 1761–1770, http://dx.doi.org/10.13031/trans.57.10781.

Boreddy, S.R., Thippareddi, H., Froning, G., Subbiah, J., 2016. Novel radiofrequency-assisted thermal processing improves the gelling properties of standard egg white powder. J. Food Sci. 81, E665–E671, http://dx.doi.org/10.1111/1750-3841.13239.

Chen, J., Pitchai, K., Birla, S., Gonzalez, R., Jones, D., Subbiah, J., 2013. Temperature-dependent dielectric and thermal properties of whey protein gel and mashed potato. Trans. ASABE 56, 1457–1467, http://dx.doi.org/10.13031/trans.56.10314.

Chen, J., Pitchai, K., Birla, S., Negahban, M., Jones, D., Subbiah, J., 2014. Heat and mass transport during microwave heating of mashed potato in domestic oven—model development, validation, and sensitivity analysis. J. Food Sci. 79, 1991–2004.

Chen, J., Pitchai, K., Jones, D., Subbiah, J., 2015. Effect of decoupling electromagnetics from heat transfer analysis on prediction accuracy and computation time in modeling microwave heating of frozen and fresh mashed potato. J. Food Eng. 144, 45–57, http://dx.doi.org/10.1016/j.jfoodeng.2014.07.013.

Chen, L., Huang, Z., Wang, K., Li, W., Wang, S., 2016a. Simulation and validation of radio frequency heating with conveyor movement. J. Electromagn. Waves Appl. 30, 473–491, http://dx.doi.org/10.1080/09205071.2015.1121841.

Chen, J., Pitchai, K., Birla, S., Jones, D., Negahban, M., Subbiah, J., 2016b. Modeling heat and mass transport during microwave heating of frozen food rotating on a turntable. Food Bioprod. Process. 99, 116–127, http://dx.doi.org/10.1016/j.fbp.2016.04.009.

COMSOL Multiphysics, 2015. Material Library V5.2. COMSOL Multiphysics.

Datta, A.K., Anantheswaran, R.C., 2001. Handbook of Microwave Technology for Food Applications. Marcel Dekker, Inc., New York.

Fiore, A., Di Monaco, R., Cavella, S., Visconti, A., Karneili, O., Bernhardt, S., Fogliano, V., 2013. Chemical profile and sensory properties of different foods cooked by a new radiofrequency oven. Food Chem. 139, 515–520, http://dx.doi.org/10.1016/j.foodchem.2013.01.028.

Guan, D., Cheng, M., Wang, Y., Tang, J., 2004. Dielectric properties of mashed potatoes relevant to microwave and radio-frequency pasteurization and sterilization processes. J. Food Sci. 69, 30–37.

Hou, L., Ling, B., Wang, S., 2014. Development of thermal treatment protocol for disinfesting chestnuts using radio frequency energy. Postharvest Biol. Technol. 98, 65–71, http://dx.doi.org/10.1016/j.postharvbio.2014.07.007.

Hou, L., Hou, J., Li, Z., Johnson, J.A., Wang, S., 2015. Validation of radio frequency treatments as alternative non-chemical methods for disinfesting chestnuts. J. Stored Prod. Res. 63, 75–79, http://dx.doi.org/10.1016/j.jspr.2015.07.004.

Huang, Z., Chen, L., Wang, S., 2015a. Computer simulation of radio frequency selective heating of insects in soybeans. Int. J. Heat Mass Transf. 90, 406–417, http://dx.doi.org/10.1016/j.ijheatmasstransfer.2015.06.071.

Huang, Z., Zhu, H., Yan, R., Wang, S., 2015b. Simulation and prediction of radio frequency heating in dry soybeans. Biosyst. Eng. 129, 34–47, http://dx.doi.org/10.1016/j.biosystemseng.2014.09.014.

Jeong, S.-G., Kang, D.-H., 2014. Influence of moisture content on inactivation of *Escherichia coli* O157:H7 and *Salmonella enterica* serovar Typhimurium in powdered red and black pepper spices by radio-frequency heating. Int. J. Food Microbiol. 176, 15–22, http://dx.doi.org/10.1016/j.ijfoodmicro.2014.01.011.

Jiao, S., Johnson, J.A., Tang, J., Wang, S., 2012. Industrial-scale radio frequency treatments for insect control in lentils. J. Stored Prod. Res. 48, 143–148, http://dx.doi.org/10.1016/j.jspr.2011.12.001.

Jiao, Y., Tang, J., Wang, S., 2014. A new strategy to improve heating uniformity of low moisture foods in radio frequency treatment for pathogen control. J. Food Eng. 141, 128–138, http://dx.doi.org/10.1016/j.jfoodeng.2014.05.022.

Jiao, S., Deng, Y., Zhong, Y., Wang, D., Zhao, Y., 2015. Investigation of radio frequency heating uniformity of wheat kernels by using the developed computer simulation model. Food Res. Int. 71, 41–49, http://dx.doi.org/10.1016/j.foodres.2015.02.010.

Johnson, J.A., Valero, K.A., Wang, S., Tang, J., 2004. Thermal death kinetics of red flour beetle (Coleoptera: Tenebrionidae). J. Econ. Entomol. 97.

Kim, S.-Y., Sagong, H.-G., Choi, S.H., Ryu, S., Kang, D.-H., 2012. Radio-frequency heating to inactivate *Salmonella typhimurium* and *Escherichia coli* O157:H7 on black and red pepper spice. Int. J. Food Microbiol. 153, 171–175, http://dx.doi.org/10.1016/j.ijfoodmicro.2011.11.004.

Laycock, L., Piyasena, P., Mittal, G.S., 2003. Radio frequency cooking of ground, comminuted and muscle meat products. Meat Sci. 65, 959–965, http://dx.doi.org/10.1016/S0309-1740(02)00311-X.

Liu, S., Fukuoka, M., Sakai, N., 2013. A finite element model for simulating temperature distributions in rotating food during microwave heating. J. Food Eng. 115, 49–62, http://dx.doi.org/10.1016/j.jfoodeng.2012.09.019.

Mitcham, E., Veltman, R., Feng, X., de Castro, E., Johnson, J., Simpson, T., Biasi, W., Wang, S., Tang, J., 2004. Application of radio frequency treatments to control insects in in-shell walnuts. Postharvest Biol. Technol. 33, 93–100, http://dx.doi.org/10.1016/j.postharvbio.2004.01.004.

Pitchai, K., Chen, J., Birla, S., Gonzalez, R., Jones, D., Subbiah, J., 2014. A microwave heat transfer model for a rotating multi-component meal in a domestic oven: development and validation. J. Food Eng. 128, 60–71.

Pitchai, K., Chen, J., Birla, S., Jones, D., Gonzalez, R., Subbiah, J., 2015a. Multiphysics modeling of microwave heating of a frozen heterogeneous meal rotating on a turntable. J. Food Sci. 80, E2803–E2814, http://dx.doi.org/10.1111/1750-3841.13136.

Pitchai, K., Chen, J., Birla, S., Jones, D., Subbiah, J., 2015b. Modeling microwave heating of frozen mashed potato in a domestic

oven incorporating electromagnetic frequency spectrum. J. Food Eng. 173, 124–131, http://dx.doi.org/10.1016/j.jfoodeng.2015.11.002.
Romano, V., Marra, F., 2008. A numerical analysis of radio frequency heating of regular shaped foodstuff. J. Food Eng. 84, 449–457, http://dx.doi.org/10.1016/j.jfoodeng.2007.06.006.
Schlisselberg, D.B., Kler, E., Kalily, E., Kisluk, G., Karniel, O., Yaron, S., 2013. Inactivation of foodborne pathogens in ground beef by cooking with highly controlled radio frequency energy. Int. J. Food Microbiol. 160, 219–226, http://dx.doi.org/10.1016/j.ijfoodmicro.2012.10.017.
Shrestha, B., Baik, O.-D., 2013. Radio frequency selective heating of stored-grain insects at 27.12 MHz: a feasibility study. Biosyst. Eng. 114, 195–204, http://dx.doi.org/10.1016/j.biosystemseng.2012.12.003.
Sipahioglu, O., Barringer, S.A., 2003. Dielectric properties of vegetables and fruits as a function of temperature, ash, and moisture content. J. Food Sci. 68, 234–239.
Tang, X., Cronin, D., Brunton, N., 2005. The effect of radio frequency heating on chemical, physical and sensory aspects of quality in turkey breast rolls. Food Chem. 93, 1–7, http://dx.doi.org/10.1016/j.foodchem.2004.08.037.
Tang, J., Mitcham, E., Wang, S., Lurie, S., 2007. Heat Treat. Postharvest Pest Control Theory Pract. CABI.
Tiwari, G., Wang, S., Tang, J., Birla, S.L., 2011a. Analysis of radio frequency (RF) power distribution in dry food materials. J. Food Eng. 104, 548–556, http://dx.doi.org/10.1016/j.jfoodeng.2011.01.015.
Tiwari, G., Wang, S., Tang, J., Birla, S.L., 2011b. Computer simulation model development and validation for radio frequency (RF) heating of dry food materials. J. Food Eng. 105, 48–55, http://dx.doi.org/10.1016/j.jfoodeng.2011.01.016.
Uyar, R., Erdogdu, F., Marra, F., 2014. Effect of load volume on power absorption and temperature evolution during radio-frequency heating of meat cubes: a computational study. Food Bioprod. Process. 92, 243–251, http://dx.doi.org/10.1016/j.fbp.2013.12.005.
Uyar, R., Bedane, T.F., Erdogdu, F., Koray Palazoglu, T., Farag, K.W., Marra, F., 2015. Radio-frequency thawing of food products—a computational study. J. Food Eng. 146, 163–171, http://dx.doi.org/10.1016/j.jfoodeng.2014.08.018.
Wang, S., Ikediala, J., Tang, J., Hansen, J., Mitcham, E., Mao, R., Swanson, B., 2001. Radio frequency treatments to control codling moth in in-shell walnuts. Postharvest Biol. Technol. 22, 29–38, http://dx.doi.org/10.1016/S0925-5214(00)00187-3.
Wang, S., Birla, S.L., Tang, J., Hansen, J.D., 2006. Postharvest treatment to control codling moth in fresh apples using water assisted radio frequency heating. Postharvest Biol. Technol. 40, 89–96, http://dx.doi.org/10.1016/j.postharvbio.2005.12.005.
Wang, S., Monzon, M., Johnson, J.A., Mitcham, E.J., Tang, J., 2007. Industrial-scale radio frequency treatments for insect control in walnuts I: heating uniformity and energy efficiency. Postharvest Biol. Technol. 45, 240–246, http://dx.doi.org/10.1016/j.postharvbio.2006.12.023.
Wang, J., Luechapattanaporn, K., Wang, Y., Tang, J., 2012. Radio-frequency heating of heterogeneous food—meat lasagna. J. Food Eng. 108, 183–193, http://dx.doi.org/10.1016/j.jfoodeng.2011.05.031.
Wang, S., Tang, J., Johnson, J.A., Cavalieri, R.P., 2013. Heating uniformity and differential heating of insects in almonds associated with radio frequency energy. J. Stored Prod. Res. 55, 15–20, http://dx.doi.org/10.1016/j.jspr.2013.06.003.